Energy Conversion and Management 76 (2013) 712–724

Contents lists available at ScienceDirect

Energy Conversion and Management

journal homepage: www.elsevier.com/locate/enconman

Simulation of a heavy-duty diesel engine with electrical turbocompounding system using operating charts for turbocharger components and power turbine

C.O. Katsanos [a], D.T. Hountalas [a], T.C. Zannis [b,*]

[a] Thermal Engineering Section, School of Mechanical Engineering, National Technical University of Athens, 9 Heroon Polytechniou St., Zografou Campus, 157 80 Athens, Greece
[b] Section of Naval Architecture & Marine Engineering, Hellenic Naval Academy, End of Hatzikiriakou Ave., 18539 Piraeus, Greece

ARTICLE INFO

Article history:
Received 26 February 2013
Accepted 5 August 2013

Keywords:
Diesel engine
Electrical turbocompounding
Turbocharger
Operating charts

ABSTRACT

In diesel engines, approximately 30–40% of the energy supplied by the fuel is rejected to the ambience through exhaust gases. Therefore, there is a potentiality for further considerable increase of diesel engine efficiency with the utilization of exhaust gas heat and its conversion to mechanical or electrical energy. In the present study, the operational behavior of a heavy-duty (HD) diesel truck engine equipped with an electric turbocompounding system is examined on a theoretical basis. The electrical turbocompounding configuration comprised of a power turbine coupled to an electric generator, which is installed downstream to the turbocharger (T/C) turbine. A diesel engine simulation model has been developed using operating charts for both turbocharger and power turbine. A method for introducing the operating charts into the engine model is described thoroughly. A parametric analysis is conducted with the developed simulation tool, where the varying parameter is the rotational speed of power turbine shaft. In this study, the interaction between the power turbine and the turbocharged diesel engine is examined in detail. The effect of power turbine speed on T/C components efficiencies, power turbine efficiency, exhaust pressure and temperature, engine boost pressure and air to fuel ratio is evaluated. In addition, theoretical results for the potential impact of electrical turbocompounding on the generated electric power, net engine power and relative improvement of brake specific fuel consumption (bsfc) are provided. The critical evaluation of the theoretical findings led to the basic conclusion that there is a significant potential for bsfc improvement of HD diesel truck engines with the proposed electrical turbocompounding concept, which reaches up to 4% at full engine load. The improvement of bsfc with electric turbocompounding appears to be more attractive solution in terms of technical complexity and installation cost against other competitive heat recovery technologies such as Rankine cycle systems.

1. Introduction

Diminishing petroleum supplies and increasing fuel cost have motivated diesel engine manufacturers and engineers to improve fuel economy. During recent years, various in-cylinder technologies have been implemented to increase further diesel engine efficiency and thus, to curtail CO_2 emissions and simultaneously to reduce further diesel-emitted gaseous and particulate pollutants [1,2]. During the last decade, the in-cylinder measures used to improve conventional diesel engine efficiency and polluting behavior have been primarily focused on the manipulation of fuel injection process (i.e. increase of fuel injection pressure, variation of fuel injection timing and rate and application of multiple injection events) and on the development and implementation of advanced turbocharging systems [3–6]. Towards a further improvement of the operational and environmental behavior of diesel engines, alternative low temperature combustion (LTC) strategies such as Homogeneous Charge Compression Ignition (HCCI), Premixed Charge Compression Ignition (PCCI) and Reactivity Controlled Compression Ignition (RCCI) have been examined both theoretically and experimentally during recent years [1,2]. The application of the aforementioned LTC techniques in diesel engine generated quite promising results mainly in the field of simultaneous reduction of soot and NOx emissions, which are the pollutants of primary interest in diesel engines.

However, the application of the aforementioned in-cylinder measures and advanced LTC technologies has not succeeded in providing remarkable improvements of diesel engine brake efficiency. For this reason, during recent years, research community has been intensively focused on the improvement of diesel cycle management. According to diesel cycle principles, a significant

* Corresponding author. Tel.: +30 2104581663; fax: +30 2104581334.
E-mail address: tczannis@gmail.com (T.C. Zannis).

0196-8904/$ - see front matter © 2013 Elsevier Ltd. All rights reserved.
http://dx.doi.org/10.1016/j.enconman.2013.08.022

Nomenclature

$\dot{m}$	flow rate (kg/s)
$\dot{N}$	rotational speed (r/min)
A	area (m^2)
a_{del}	ignition delay constant
C_0	mass fraction of oxygen
c_d	discharge coefficient
C_f	mass fraction of fuel
c_p	constant pressure thermal heat capacity (J/kg K)
d_{inj}	injector hole diameter (m)
E	activation energy (J/kmol)
$EFF_{T/C}$	turbocharger efficiency
h	heat transfer coefficient (W/m^2 K)
K_b	combustion rate constant
l_{car}	characteristic length (m)
m	mass (kg)
n_{compr}	compressor isentropic efficiency
n_{mTC}	turbocharger isentropic efficiency
p	pressure (bar)
Power	power (W)
$Power_{frTC}$	frictional power loss in turbocharger shaft (W)
Pr	Prandtl number
Re	Reynolds number
R_{mol}	universal gas constant (J/kmolK)
S_{pr}	ignition delay integral
T	temperature (K)
t	time (s)
t_b	break up time (s)
t_{hit}	time of impingement (s)
u	velocity (m/s)
u_p	penetration velocity (m/s)

Greek symbols

γ	Isentropic exponent
Δp	pressure difference (Pa)
ε_t	viscous dissipation rate per unit mass (W/kg)
η	efficiency
λ	thermal conductivity (W/m K)
ρ	density (kg/m^3)
Φ_{eq}	equivalence ratio

Subscripts

air	air
compr	compressor
COR	corrected value
del	delay
ET	electrical turbocompounding
f	fuel
g	gas
GEN	generated
in	inlet
inj	injection
l	liquid fuel
p	penetration
ST	standard engine operation
TC	turbocharger
turb	turbine

Abbreviations

ATDC	after top dead center
bmep	brake mean effective pressure
bsfc	brake specific fuel consumption
CA	crank angle
CAC	charge air cooler
EGR	exhaust gas recirculation
HCCI	homogeneous charge compression ignition
HD	heavy duty
LTC	low temperature combustion
NOx	nitrogen oxides
ORC	organic Rankine cycle
PCCI	premixed charge compression ignition
RCCI	reactivity controlled compression ignition
SRC	steam Rankine cycle
T/C	turbocharger, turbocharged
TEG	thermoelectric generator
WHR	waste heat recovery

amount of fuel supplied energy is not transformed into useful mechanical power and it is rejected to the ambience as exhaust heat. In existing diesel engines, the unexploited waste heat reaches up to 30–40% of the feeding fuel energy. Hence, potentiality for significant improvement of diesel engine efficiency is envisaged through the utilization of exhaust energy for additional power generation.

Recent review studies [7–11] examined thoroughly the implementation of various waste heat recovery (WHR) technologies on both theoretical and experimental basis and demonstrated the individual impact of each technology on the improvement of brake specific fuel consumption (bsfc) and on the operability of modern diesel engines under steady-state and transient operation. The aforesaid WHR strategies can be effectively implemented in various applications of diesel engines such as transportation vehicles, marine propulsion and electric power generation [11–15]. Especially, in the field of heavy-duty (HD) diesel engines, which are used as prime movers of trucks, the dominating WHR technologies are the following:

1.1. Mechanical turbocompounding

This WHR technology involves the installation of a power turbine after the turbocharger (T/C) turbine for extracting mechanical power from the exhaust gas stream. Studies conducted in the past mainly by engine manufacturers have shown that the implementation of mechanical turbocompounding in HD diesel engines may result in considerable bsfc improvement [16–23]. Specifically, Leising et al. [16] examined the installation of an axial power turbine downstream to the T/C turbine of a 14.6-L diesel engine and they reported an average bsfc reduction of about 4.7% for a 50,000 miles extra-urban driving test in the US. Tennant and Walsham [19] implemented mechanical turbocompounding on an 11-L 6-cylinder T/C diesel engine and they reported a 5% bsfc improvement at full load.

1.2. Electrical turbocompounding

The concept of this strategy is based on the coupling of an electrical generator to the T/C shaft for extracting excess power produced from the turbine. In this case, the turbine produces more power compared to the one required to drive the compressor. The excess power is converted to electric power using a high speed generator incorporated into the T/C casing. Earlier studies performed on the field of electrical turbocompounding have demonstrated that the application of this WHR technology in HD diesel engines may achieve comparable or higher bsfc reductions compared to the aforementioned mechanical turbocompounding

concept [21,24–26]. Specifically, experimental studies performed in the past by an engine development company [25,26] have shown the implementation of electrical turbocompounding in a HD diesel truck engine can result in 5% reduction of bsfc on a cycle basis and in a maximum bsfc improvement of approximately 9–10% when using T/C components with high efficiency.

1.3. Rankine cycle system

This technology is based on the installation of a Rankine bottoming cycle system, which operates using either steam or organic fluid (ORC) as working medium, for generating additional power through a reciprocating expander or in most cases, a turbine [7–15,21,27–41]. Recent theoretical and experimental studies, which examined the application of either steam Rankine cycle (SRC) or ORC system and they were performed considering heat extraction not only from exhaust gases but also from the exhaust gas recirculation (EGR) system and the charge air cooler (CAC), have shown that the maximum bsfc improvement can reach up to 9% in the case of SRC and up to 11% in the case of ORC [35,36,39]. Leading engine manufacturers have reported lately that they have developed HD diesel engines for truck applications with 50% brake thermal efficiency and they are planning to increase it up to 55% in 2014 using various Rankine cycle configurations [40,41].

1.4. Thermoelectric generator

This WHR technology is based on the direct conversion of exhaust gas heat to electric power using thermoelectric phenomenon. According to previous studies [21,42,43] the application of thermoelectric generators (TEG) has produced relatively lower improvements in overall diesel efficiency compared to the aforementioned WHR technologies. However, the continuous evolution of thermoelectric materials in terms of generated electric power can make this technology more attractive for future HD diesel truck engine applications.

According to the examined literature, mechanical and electrical turbocompounding appear to be attractive solutions for heat recovery in diesel engines. The advantages of the turbocompounding concepts compared to Rankine cycle system are the relatively lower complexity, size, weight and cost. However, the main disadvantage of turbocompounding technology is the increase of the engine back-pressure and pumping losses that result to the reduction of net engine power. For the case of electrical turbocompounding, the increase of the turbine inlet pressure is limited because it results in a significant increase of the pressure ratio across the turbine. Thus, the existence of a power turbine downstream to the T/C turbine seems to be the more attractive solution.

The optimum configuration for the turbocompounding technique is a combination of the electrical and mechanical concept. Specifically, an electric generator coupled to the power turbine replaces the gear train in mechanical turbocompounding to reduce volume and mechanical losses. A representative schematic view of the proposed turbocompounding technology, which is examined in the present paper, is shown in Fig. 1.

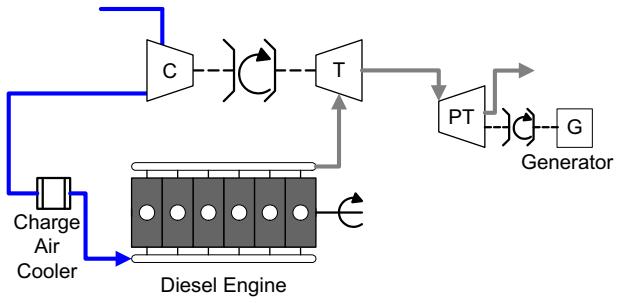

Fig. 1. Schematic view of electrical turbocompounding configuration considered in the present study.

Hence, a theoretical study is conducted herein to estimate the potential for exhaust gas energy recovery of a heavy-duty diesel engine using electrical turbocompounding. In pertinent studies conducted in the past [16–20,22], the varying parameter for the conducted analysis of the turbocompounding technique was the expansion ratio of the power turbine. Unlike these previously published studies, the varying parameter in the present analysis is the power turbine speed and thus the expansion ratio is calculated from the simulation model. Moreover, the present parametric study is conducted using a diesel engine simulation model, which has been appropriately modified for considering the turbocompounding technology. Operational charts have been provided by the manufacturer for compressor, turbocharger turbine and power turbine. The developed simulation model includes the previous operational charts in order to estimate the interaction between power turbine, turbocharger and diesel engine. Therefore, the present analysis is based on a more realistic simulation model compared to other studies conducted in the past [16–20,22].

The examination of the theoretical results initiates with the evaluation of the effect of turbocompounding technology on engine back-pressure and power turbine expansion ratio. Further on, the theoretical examination sheds light on the influence of power turbine rotating speed on T/C component efficiencies and power turbine efficiency. Additionally, the effect of electric turbocompounding on engine boost pressure and air to fuel ratio is elaborated for better understanding the impact of turbocompounding system on engine charge air availability. Moreover, the relative impact of electrical turbocompounding on exhaust gas pressure and temperature is elaborated. Finally, the effect of power turbine speed on generated electric power and net engine power is examined facilitating thus, the comprehension of the pertinent effect of electric power turbine on bsfc improvement.

The assessment of the theoretical results clearly indicates that the potentiality for recovering exhaust heat and converting it into useful electrical energy is quite satisfying. This is based on the fact that the implementation of electrical turbocompounding in a HD diesel truck engine resulted in bsfc reduction of approximately 4% at full load and of approximately 2% at part load. Considering continuously increasing oil prices, it appears that the proposed electrical turbocompounding system can be considered as promising solution for further bsfc improvement of HD diesel engines compared to other competitive WHR technologies such as Rankine cycle systems.

2. Description of the simulation model of the diesel engine installation with electrical turbocompounding

2.1. Brief outline of the diesel engine simulation model

The simulation code of the diesel engine is based on a three-dimensional multi-zone combustion model. The pressure inside the engine cylinder is considered to be uniform. The first law of thermodynamics and the conservation equations for mass and momentum are employed for the calculation of local conditions inside each zone. Details concerning the diesel engine simulation code have been published in the past [4,5,44] and thus only a brief description of the main mechanisms involved in the simulation model is given herein for the sake of completeness.

2.2. Description of engine simulation submodels

2.2.1. Heat transfer

A turbulent kinetic energy viscous dissipation rate $k \sim \varepsilon_t$ model is used to determine the characteristic velocity for the heat transfer calculations [45]. The heat transfer coefficient is estimated from the following correlation [46]:

$$h_c = c\mathrm{Re}^{0.8}\mathrm{Pr}^{0.33}\frac{\lambda}{l_{\mathrm{car}}} \tag{1}$$

The overall heat exchange rate is then distributed among the zones according to their mass, temperature and specific heat capacity.

2.2.2. Air swirl

The swirling motion of the intake air is described assuming a hybrid scheme consisting of a solid body core surrounded by a potential flow region [47]. The intake air swirl velocity is estimated from the angular momentum conservation equation using the angular momentum added to the engine cylinder during the intake process and considering for the part destroyed because of friction with the combustion chamber walls. Details concerning air swirl modeling can be found in [44].

2.2.3. Spray model

After initiation of fuel injection, zones form and penetrate inside the combustion chamber. The zone velocity along the jet axis is obtained from the following relations depending on the time instant after injection [48].

$$u_p = c_d\sqrt{\frac{2\Delta p}{\rho_l}} \text{ for } t < t_b \tag{2}$$

$$u_p = \frac{2.95}{2}\left(\frac{\Delta p}{\rho_a}\right)^{0.25} d_{\mathrm{inj}}^{0.5} t^{-0.5} \text{ for } t_b < t < t_{hit} \tag{3}$$

$$u_p = \frac{2.95}{2}\left(\frac{\Delta p}{\rho_a}\right)^{0.25} d_{\mathrm{inj}}^{0.5} t^{-0.5} \text{ for } t > t_{hit} \tag{4}$$

where t_b is the breakup time and t_{hit} is the time of impingement on the cylinder walls. The breakup time is obtained from Jung and Assanis [49].

$$t_b = 4.351\frac{\rho_l d_{\mathrm{inj}}}{c_d(\rho_a \Delta p)^{0.5}} \tag{5}$$

The effect of air swirl upon the jet is considered for, using the local components of the air velocity in the radial and axial directions and using the momentum conservation equations in both axes.

2.2.4. Air entrainment into the zones

The air entrained into a zone from initiation of injection is calculated from the conservation of momentum using the following relation:

$$m_f \cdot u_{\mathrm{inj}} = (m_a + m_f)\cdot u_p \rightarrow m_a = (m_f \cdot u_{\mathrm{inj}}/u_p - m_f) \tag{6}$$

2.2.5. Droplet break up and evaporation

The injected fuel is distributed to the zones according to the instantaneous injection rate, while inside each zone the fuel is divided into packages (groups) using a chi-squared distribution [48,50], where the droplets have the same Sauter Mean Diameter. For evaporation the model of Borman and Johnson [51] is adopted, as described in [44].

2.2.6. Combustion model

The amount of air entering a zone is mixed with evaporated fuel. The local reaction rate depends on the local mass concentration of fuel, oxygen and the local temperature. Ignition commences after an ignition delay period, which is estimated using the local conditions inside the zone as follows [52]:

$$S_{\mathrm{pr}} = \int_0^1 \frac{1}{a_{\mathrm{del}} p_g^{-2.5} \Phi_{\mathrm{eq}}^{-1.04} \exp(5000/T_g)} dt = 1 \tag{7}$$

where "Φ_{eq}" is the local equivalence ratio of the fuel–air mixture inside the zone and a_{del} is a constant. After ignition the fuel combustion rate is calculated using the following relation:

$$m_{\mathrm{fb}} = K_b C_f^{\mathrm{af}} C_o^{\mathrm{ao}} \exp\left(-\frac{E_c}{R_m}\right)\frac{1}{6N} \tag{8}$$

where K_b is a constant, E_c the activation energy and C_f, C_o the mass concentrations of fuel and oxygen respectively. During diffusion phase of combustion, the combustion rate is practically controlled from the air entrainment rate and its mixing with evaporated fuel.

2.2.7. Fuel injection

The fuel injection system is of great importance for the operation of the diesel engine. In the present work, the injection rate has been obtained from the following relation:

$$\frac{dm_{\mathrm{inj}}}{dt} = C_{\mathrm{dinj}} \cdot A_{\mathrm{inj}} \cdot \sqrt{2 \cdot \Delta p \cdot \rho_f} \tag{9}$$

where $\Delta p = p_{\mathrm{cyl}} - p_{\mathrm{inj}}$ is the instantaneous pressure difference at the nozzle exit, C_{dinj} is the discharge coefficient, A_{inj} is the area of the nozzle holes and ρ_f is the fuel density. Since experimental injection rates were not available a constant rail pressure has been used during injection, which was estimated in order predicted injection duration to match the measured one at each operating condition.

2.2.8. Gas exchange

For the simulation of the inlet and exhaust manifolds and the calculation of the mass exchange rate between them and the engine cylinder the filling and emptying method is used [53]. One-dimensional, quasi-steady, compressible flow is assumed for the calculation of the mass flow rates through the inlet and exhaust valves during the gas exchange process.

2.3. Compressor simulation

The simulation of compressor is based on two different operating charts. The first chart is a diagram of the boost pressure variation with the corrected value of mass flow rate, where the corrected value of turbocharger speed is a parameter. The corrected value of mass flow rate $\dot{m}_{compr}^{COR}$ is provided from the following expression:

$$\dot{m}_{\mathrm{compr}}^{\mathrm{COR}} = \frac{\dot{m}_{\mathrm{compr}}\sqrt{T_{\mathrm{air,in}}}}{0.10 \cdot p_{\mathrm{boost}}} \tag{10}$$

The corrected value of turbocharger rotational speed is estimated as follows:

$$\dot{N}_{\mathrm{TC,compr}}^{\mathrm{COR}} = \frac{\dot{N}_{\mathrm{TC}}}{\sqrt{T_{\mathrm{air,in}}}} \tag{11}$$

The second operating chart of compressor is a diagram of compressor efficiency variation with mass flow rate for various values of corrected speed.

The calculation procedure for compressor initiates with the first operating chart. The operating point is estimated from the independent variables of boost pressure and corrected mass flow rate. The iso-value curve passing through the operating point is

calculated and the corresponding value of turbocharger speed is predicted.

Each iso-value curve of the operating charts corresponds to a specific corrected value of speed. Surge and choke lines designate the operating range for air mass flow rate. In the operating charts of compressor, all the curves are described with fifth degree polynomials. The operating chart of boost pressure is divided into six subregions, as it is shown in Fig. 2:

- The first subregion is designated from surge line, choke line and the operating curves corresponding to the maximum and minimum speed values.
- The second region contains the operating points corresponding to mass flow rate values out of the operating range of compressor.
- The third subregion contains the operating points with boost pressure values greater than the corresponding ones of surge line.
- The fourth subregion corresponds to the area located below the curve of minimum speed value.
- The fifth subregion includes the area above the curve of maximum speed value.
- The last subregion contains all the operating points below the choke line.

As revealed in Fig. 2, compressor operating points should be placed in the first subregion. When the operating point is placed on a specified iso-value curve the corresponding value of compressor speed is estimated directly. In most cases the estimated operating point by the simulation model is placed between two sequential iso-value curves. The estimation of compressor rotational speed is based on the following relation:

$$\dot{N}^{COR}_{TC,compr} = \left(\frac{D_1}{D_1 + D_2}\right)\dot{N}^{COR}_{TC,compr2} + \left(\frac{D_2}{D_1 + D_2}\right)\dot{N}^{COR}_{TC,compr1} \quad (12)$$

where D_1 is the distance between point A and compressor operating point K, D_2 is the distance between point B and operating point K, $\dot{N}^{COR}_{TC,compr1}$ and $\dot{N}^{COR}_{TC,compr2}$ are the values of corrected speed corresponding to the sequential iso-value curves. As shown in Fig. 2, the simulation model creates an imaginable straight line, which is parallel to the surge line and passes through the operating point. Points A and B are the intersection of the straight line with the sequential iso-value curves respectively. When one of the aforementioned intersection points is located outside from compressor operating region then the previous calculation procedure is modified. In this case, the updated imaginable straight line is parallel to the choke line and the intersection points are A′ and B′, as depicted in Fig. 2. After the estimation of the turbocharger rotational speed, the simulation procedure continues with the calculation of compressor efficiency using the corresponding operating map. Specifically, compressor efficiency is estimated from the values of turbocharger speed and mass flow rate.

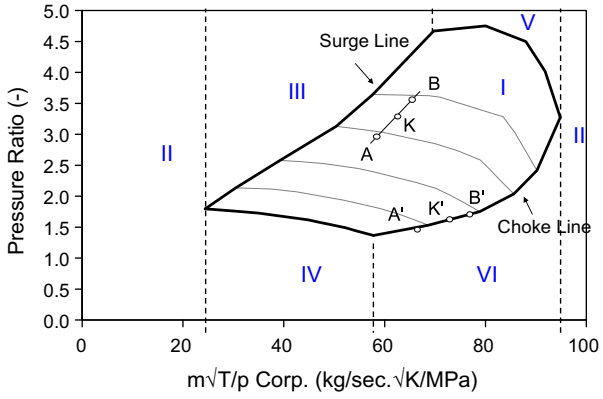

Fig. 2. Compressor operating chart showing the variation of boost pressure as a function of corrected air mass flow rate. The calculation procedure followed by the simulation model is also shown.

2.4. Turbocharger turbine and power turbine simulation

The simulation of turbocharger turbine and power turbine is based on two different operating charts. The first operating chart is the variation of corrected mass flow rate with the increase of corrected rotational speed for various values of expansion ratio. The second operating chart contains the curves of the efficiency variation with corrected turbine speed for each expansion ratio value. Thus, the parameter of these operating charts is the expansion ratio across the turbine.

Corrected values of mass flow rate $\dot{m}^{COR}_{turb}$ and turbine speed $\dot{N}^{COR}_{TC,turb}$ are provided from the following equations:

$$\dot{m}^{COR}_{turb} = \frac{\dot{m}_{turb}\sqrt{T_{exh,in}}}{0.10 \cdot p_{exh,in}} \quad (13)$$

$$\dot{N}^{COR}_{TC,turb} = \frac{\dot{N}_{TC}}{\sqrt{T_{exh,in}}} \quad (14)$$

For power turbine simulation, the previous equations are modified with the introduction of the corresponding values of mass flow rate, exhaust temperature, exhaust pressure and power turbine speed $\dot{N}_{PT}$. It is obvious that the exhaust gas mass flow rate is the same at the entrances of T/C turbine and power turbine. Furthermore, the corrected value of power turbine mass flow rate is higher than the corresponding value of T/C turbine considering that the expansion ratio at T/C turbine is lower than values for both turbines.

2.4.1. Mechanical losses of turbocharger shaft

Turbocharger mechanical efficiency is estimated from the following expression:

$$n_{mTC} = 1 - \frac{\text{Power}_{frTC}}{\text{Power}_{turb}} \quad (15)$$

where the mechanical power losses of the turbocharger shaft Power_{frTC} are calculated from the expression:

$$\text{Power}_{frTC} = c_1 + c_2\dot{N}_{TC} + c_3\dot{N}^2_{TC} \quad (16)$$

The constants c_1, c_2, c_3 of the previous expression are estimated from the corresponding experimental values of the turbocharger speed, the generated power at the turbocharger turbine and the required power for compressor. The mechanical power loss of the turbocharger is the difference between the produced turbine power and the required power for compressor. Thus, a second degree polynomial interpolation is applied to fit the experimental data points of the turbocharger speed and the mechanical power losses. As a result, the coefficients of the previous expression for mechanical power losses are: $c_1 = -4339.1$, $c_2 = 72.068$, $c_3 = 0.3819$.

2.5. Description of turbocharger simulation model

The simulation process initiates with the selection of a random operating point for the compressor. Therefore, initial values for boost pressure, air mass flow rate, compressor efficiency and turbocharger speed are defined.

During the calculation procedure, the exhaust gas mass flow rate entering the T/C turbine is calculated at each time-step from

the corresponding operating chart. In addition, the T/C turbine efficiency is also estimated from the corresponding efficiency chart. The corrected values of mass flow rate and speed are calculated from Eqs. (13) and (14) at each time step, where the exhaust pressure and temperature values correspond to the previous time-step.

The calculation procedure continues with the simulation of power turbine and the methodology is the same with the turbocharger turbine except from the fact that power turbine speed is a varying parameter.

The energy equilibrium and continuity law for the turbocharger are provided from the following expressions respectively:

$$\text{Power}_{\text{compr}} = \text{Power}_{\text{turb}} n_{\text{mTC}} \tag{17}$$

$$\dot{m}_{\text{turb}} = \dot{m}_{\text{compr}} + \dot{m}_{\text{fuel}} \tag{18}$$

When the energy equilibrium for turbocharger is not satisfied then the calculation procedure is repeated and the updated boost pressure value is provided from the following equation of the energy balance:

$$p_{\text{boost}} = \left(\frac{\text{Power}_{\text{turb}}}{\dot{m}_{\text{compr}} c_{\text{pair}} T_{\text{air,in}}} n_{\text{compr}} n_{\text{mTC}} + 1 \right)^{\frac{\gamma_{\text{air}}-1}{\gamma_{\text{air}}}} \tag{19}$$

If the continuity law is invalid for the turbocharger then the air mass flow rate is recalculated for the next operating cycle according to the following expression:

$$\dot{m}_{\text{compr}} = \dot{m}_{\text{turb}} - \dot{m}_{\text{fuel}} \tag{20}$$

where $\dot{m}_{\text{turb}}$ is exhaust gas mass flow rate of the current operating cycle. Therefore, a new operating point for compressor is estimated and the simulation continues until there is a convergence between the turbocharger operating points of two sequential engine cycles.

For the simulation of the turbocompound engine, an additional exhaust manifold is adopted, which connects the exit of turbocharger turbine with the entrance of power turbine. Therefore, the examined layout includes two exhaust manifolds corresponding to high and low pressure values.

3. Test cases examined

The diesel engine considered herein is the downsized version of a six-cylinder heavy-duty turbocharged truck engine having a bore of 125 mm, a stroke of 140 mm and compression ratio of 16.5:1. The engine is equipped with a common-rail fuel injection system, which allows the variation of both injection pressure and injection advance. In the present investigation both have been maintained at the standard level. The maximum brake mean effective pressure of the engine is 27 bar and the engine power has a maximum value of 334.13 kW at 1700 rpm engine speed. The effect of proposed turbocompounding technology on engine performance has been examined at various operating conditions. In the present analysis, the examined engine loads are: 100%, 75% and 50% at 1700 rpm engine speed. The required data for the standard engine without turbocompounding and the corresponding T/C are provided in Tables 1 and 2 respectively. For the present investigation, the fueling rate and the injection advance of the examined turbocompounded engine have been maintained the same as for the non-turbocompounded case (standard engine operation). It should be mentioned that the efficiency of the electric generator coupled to the power turbine was also assumed constant and equal to 95%.

Table 2
Operating data for the standard turbocharger.

Load (%)	Eff_{compr} (%)	Eff_{turb} (%)	N_{TC} (krpm)
100	72.0	72.0	98.84
75	73.5	73.5	89.301
50	73.0	73.0	79.191

At this point, it must be mentioned that the brake specific fuel consumption (bsfc) of the electrically turbocompounded HD diesel engine is calculated (in g/kWh) using the following relation:

$$\text{bsfc} = \frac{\dot{m}_f}{\text{Power}_{\text{NET}} + \text{Power}_{\text{GEN}}} \tag{21}$$

where $\dot{m}_f$ is the engine fuel consumption in g/h, $\text{Power}_{\text{NET}}$ is the net engine brake power output in kW and $\text{Power}_{\text{GEN}}$ is the generated electric power in kW. Hence, the percentage variations of bsfc and net engine brake power are calculated according to the following expressions:

$$\text{bsfc variation}(\%) = \frac{\text{bsfc}_{\text{ET}} - \text{bsfc}_{\text{ST}}}{\text{bsfc}_{\text{ET}}} \times 100\% \tag{22}$$

$$\text{Power}_{\text{NET}} \text{ variation}(\%) = \frac{\text{Power}_{\text{NET,ET}} - \text{Power}_{\text{NET,ST}}}{\text{Power}_{\text{NET,ST}}} \times 100\% \tag{23}$$

where bsfc_{ET} and $\text{Power}_{\text{NET,ET}}$ is the brake specific fuel consumption and the net engine power for operation with electrical turbocompounding (ET) system. In addition, bsfc_{ST} and $\text{Power}_{\text{NET,ST}}$ is the brake specific fuel consumption and the net engine power for operation without electrical turbocompounding (standard (ST) engine operation).

4. Model calibration and validation

Before examining the various exhaust energy recovery techniques with the simulation model, the simulation model has been calibrated at a selected operating point. Unfortunately no experimental data were available for turbocompounding. Therefore, model calibration was conducted by using data for the non-downsized engine version, i.e. 27 bar bmep. After calibration, the model predictive ability was assessed by comparing predicted engine performance data with experimental ones for the entire engine operating range. As revealed, the simulation predicts with adequate accuracy engine performance characteristics on the entire engine operating range which encouraged its use for the present investigation. Details for the model validation have been provided in a previous paper [21].

5. Results and discussion

In this section, the theoretical results, which were generated under the aforementioned parametric investigation, are provided. For the sake of brevity of space, predictions are given only at 1700 rpm engine speed since the corresponding results at 1300 rpm and 2100 rpm are quite similar. As already mentioned,

Table 1
Operating data for the standard engine without turbocompounding.

Load (%)	$\dot{m}_{fuel}$ (kg/h)	Injection advance (deg ATDC)	p_{boost} (bara)	AF (−)	p_{exh} (bar)	T_{exh} (°C)	Power (kW)
100	11.80	−8	3.08	24.41	2.66	585.40	334.13
75	8.90	−8	2.65	28.65	2.41	501.95	248.86
50	6.10	−7	2.23	35.11	2.24	420.20	165.91

the varying parameter of the analysis is the power turbine speed, which ranges from 60 krpm to 110 krpm and thus, all predictions derived for the operational parameters of the electrically turbocompounded diesel installation are expressed as functions of the power turbine speed.

At this point, it must be clarified that the operation of the power turbine is strongly interrelated to the performance of the T/C system and of the diesel engine. For this reason, the theoretical results are presented and discussed herein in a sequence that strives to shed light on the complex interconnections between power turbine operation, T/C components performance and diesel engine breathing, performance and efficiency.

5.1. Effect of power turbine speed on exhaust pressure at T/C turbine inlet and on power turbine expansion ratio

The effect of power turbine speed on the calculated mean exhaust pressure at T/C turbine inlet (high-pressure manifold) is shown in Fig. 3a for the electrically turbocompounded HD diesel engine at 1700 rpm and at 50%, 75% and 100% of full load. In Fig. 3a are given also the corresponding mean exhaust pressure values at the entrance of T/C turbine, which were considered during standard operation (i.e. without turbocompounding) at all loads of the examined HD diesel engine and they have also already listed in Table 1. As observed, the application of electrical turbocompounding on the specific HD diesel engine examined herein results in significant increase of mean exhaust pressure at the exhaust manifold connecting the engine with the T/C turbine. Specifically, for the case of engine operation with electrical turbocompounding, the average pressure value at the entrance of T/C turbine is 3.5 bar, 4.5 bar and 5.5 bar at 50%, 75% and 100% of full load. During operation with electrical turbocompounding, the corresponding absolute increase of T/C turbine inlet pressure compared to standard engine operation is 1.26 bar, 2.09 bar and 2.84 bar at 50%, 75% and 100% load. The average expansion ratio of the T/C turbine over the entire range of power turbine speed is 1.3, 2.0 and 2.8 at 50%, 75% and 100% load. Hence, it is observed a decrease of T/C turbine expansion ratio for the operation of the examined HD diesel engine with electric turbocompounding compared to conventional operation.

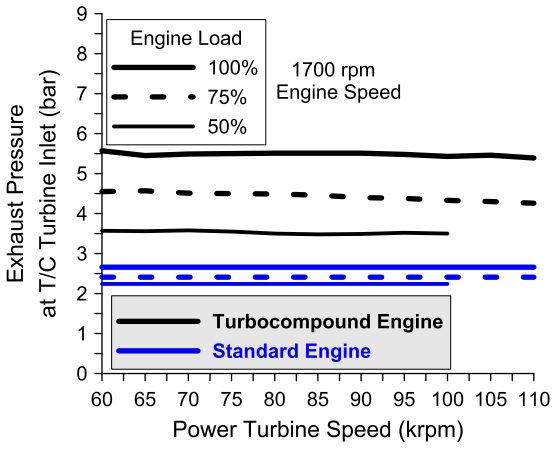

Fig. 3a. Effect of power turbine speed on mean exhaust pressure at T/C turbine inlet (high-pressure manifold). Predictions are given for an electrically turbocompounded HD diesel truck engine (black color lines) and the same engine without turbocompounding (standard case – blue color lines) at 1700 rpm and at 100%, 75% and 50% of full engine load. (For interpretation of the references to color in this figure legend, the reader is referred to the web version of this article.)

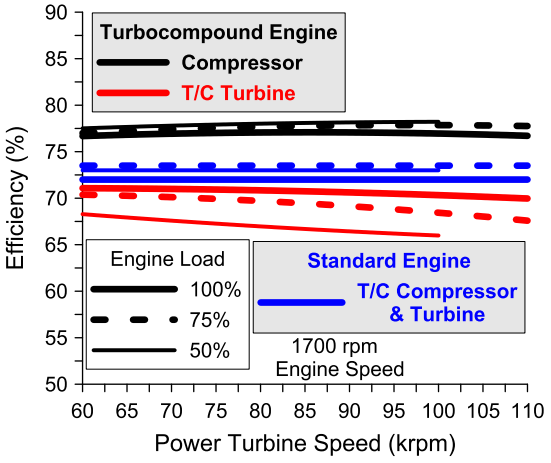

Fig. 4. Effect of power turbine speed on T/C compressor and turbine efficiencies. Predictions are given for an electrically turbocompounded HD diesel truck engine (black lines for compressor efficiency and red lines for T/C turbine efficiency) and for the same engine without turbocompounding (blue lines – standard case) at 1700 rpm and at 100%, 75% and 50% of full engine load. (For interpretation of the references to color in this figure legend, the reader is referred to the web version of this article.)

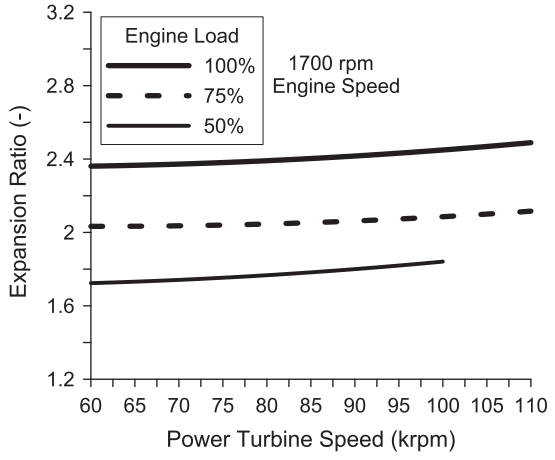

Fig. 3b. Effect of power turbine speed on its expansion ratio. Predictions are given for an electrically turbocompounded HD diesel truck engine at 1700 rpm and at 100%, 75% and 50% of full engine load.

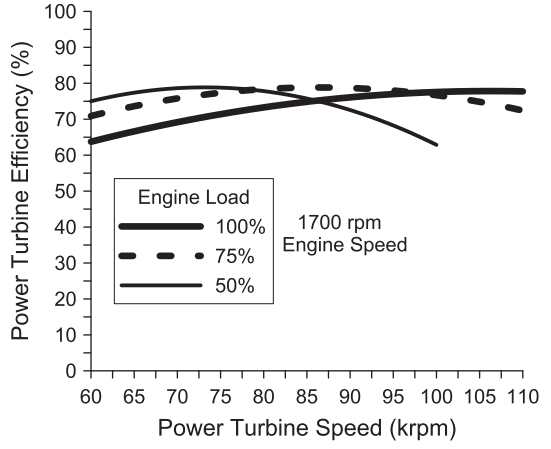

Fig. 5. Effect of the rotational speed of the power turbine on its efficiency. Predictions are given for an electrically turbocompounded HD diesel truck engine at 1700 rpm and at 100%, 75% and 50% of full engine load.

The increase of mean engine back-pressure (i.e. exhaust pressure between engine and T/C turbine inlet), which accompanied the application of turbocompounding technology, is primarily attributed to the operation of the rotational power turbine, which is opposed to the free flow of exhaust gases to the ambience. As will be shown in following paragraphs, the reduction of T/C turbine expansion ratio mainly at part loads as a result of the application of electrical turbocompounding affects directly the efficiency of the T/C turbine (Fig. 4) and thus, the rotational speed of the T/C shaft (Fig. 6). In addition, it will be shown that the increase of exhaust back-pressure and the reduction of T/C turbine expansion ratio affect directly the supply of charge air (Figs. 7a and 7b)) to the diesel engine by the T/C compressor and subsequently, affect the in-cylinder air to fuel stoichiometric analogy and the combustion efficiency and finally, the exhaust gas temperature (Fig. 8a) and the net engine power (Fig. 9b).

In Fig. 3b is presented the effect of power turbine speed on the expansion ratio of the power turbine. Theoretical results are given for the turbocompounded HD diesel engine examined in the present study at 1700 rpm and at 50%, 75% and 100% of full load. As observed, the increase of power turbine speed results in a limited increase of expansion ratio at all loads examined. Hence, it appears that the increase of rotational speed facilitates the transformation of exhaust gas thermal energy into useful mechanical power. Exhaust gases expand to the ambience in the power turbine. Hence, the values of expansion ratio correspond also to the mean exhaust pressure values at the inlet of the power turbine. These pressure values are significantly lower compared to the pertinent values observed in Fig. 3a at the entrance of the T/C turbine during turbocompounded operation. This means that the mean pressure variation between the high-pressure exhaust manifold between engine and T/C turbine and the low-pressure exhaust manifold between T/C turbine outlet and power turbine inlet is noticeable ought to the initial expansion of exhaust gas in the T/C turbine.

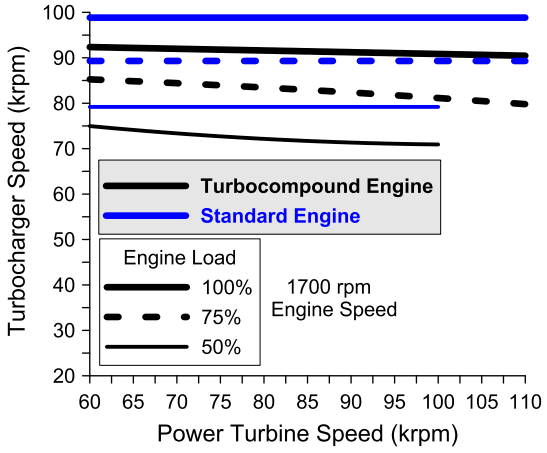

Fig. 6. Effect of power turbine speed on turbocharger rotational speed. Predictions are given for an electrically turbocompounded HD diesel truck engine (black lines) and for the same engine without turbocompounding (blue lines – standard case) at 1700 rpm and at 100%, 75% and 50% of full engine load. (For interpretation of the references to color in this figure legend, the reader is referred to the web version of this article.)

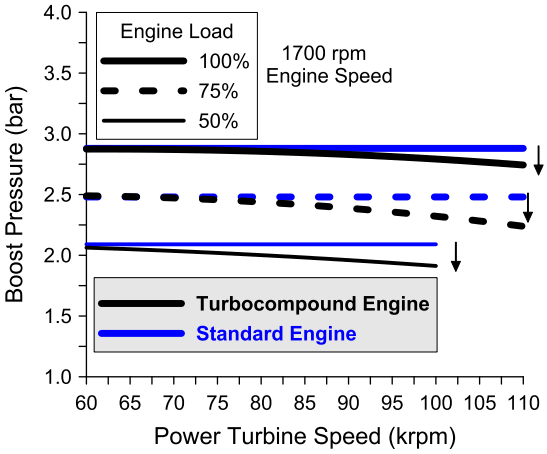

Fig. 7a. Effect of power turbine speed on engine boost pressure. Predictions are given for an electrically turbocompounded HD diesel truck engine (black lines) and for the same engine without turbocompounding (blue lines – standard case) at 1700 rpm and at 100%, 75% and 50% of full engine load. (For interpretation of the references to color in this figure legend, the reader is referred to the web version of this article.)

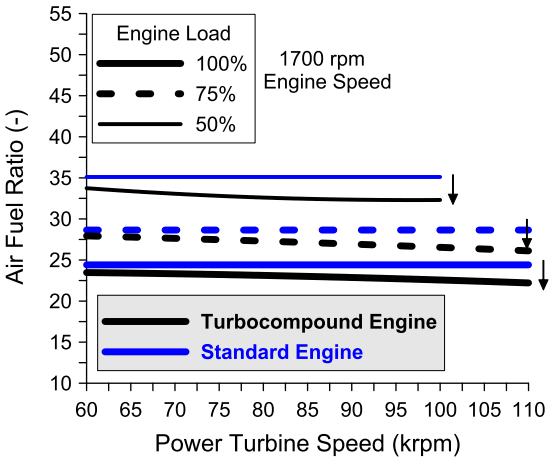

Fig. 7b. Effect of power turbine speed on average air to fuel ratio. Predictions are given for an electrically turbocompounded HD diesel truck engine (black lines) and for the same engine without turbocompounding (blue lines – standard case) at 1700 rpm and at 100%, 75% and 50% of full engine load. (For interpretation of the references to color in this figure legend, the reader is referred to the web version of this article.)

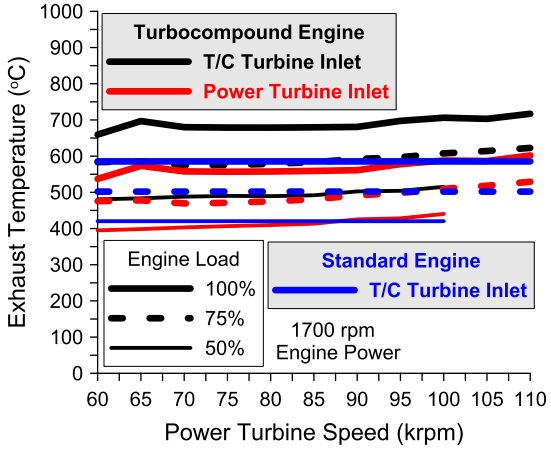

Fig. 8a. Effect of power turbine speed on the mean values of exhaust temperature at T/C turbine inlet and power turbine inlet. Predictions are given for an electrically turbocompounded HD diesel truck engine (black lines for T/C turbine inlet and red lines for power turbine inlet) and for the same engine without turbocompounding (blue lines – standard case) at 1700 rpm and at 100%, 75% and 50% of full engine load. (For interpretation of the references to color in this figure legend, the reader is referred to the web version of this article.)

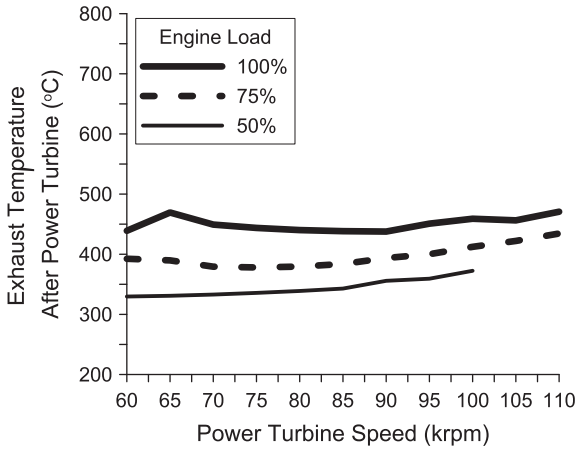

Fig. 8b. Effect of power turbine speed on the mean value of exhaust temperature after power turbine. Predictions are given for an electrically turbocompounded HD diesel truck engine at 1700 rpm and at 100%, 75% and 50% of full engine load.

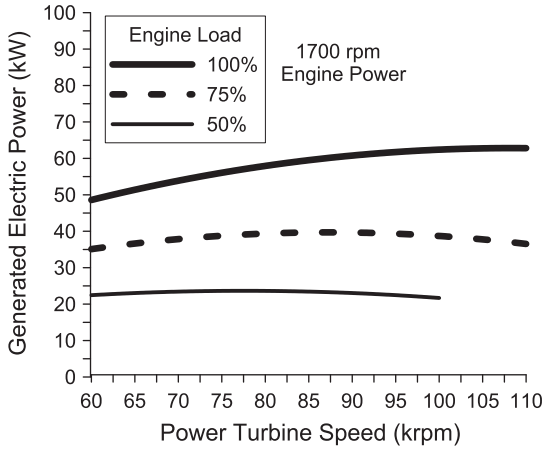

Fig. 9a. Effect of power turbine speed on generated electric power. Predictions are given for an electrically turbocompounded HD diesel truck engine at 1700 rpm and at 100%, 75% and 50% of full engine load.

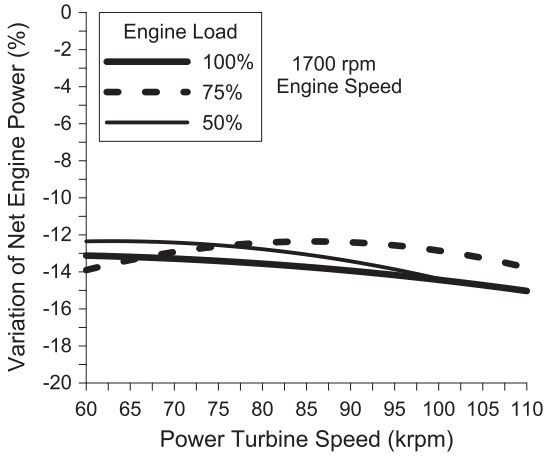

Fig. 9b. Effect of power turbine speed on the percentage variation of net engine brake power with reference to standard engine operation without turbocompounding. Predictions are given for an electrically turbocompounded HD diesel truck engine at 1700 rpm and at 100%, 75% and 50% of full engine load.

5.2. Effect of power turbine speed on T/C components efficiencies and on power turbine efficiency

The effect of turbocompounding technology on the efficiencies of compressor and T/C turbine is shown in Fig. 4. Fig. 4 also provides the case of the standard engine without turbocompounding, where compressor and T/C turbine have the same efficiency. As observed from Fig. 4, the application of electrical turbocompounding on the examined HD diesel engine results in an increase of T/C compressor efficiency and in a decrease of T/C turbine efficiency compared to the corresponding values of the standard T/C. As already mentioned in the description of compressor simulation, compressor efficiency depends on T/C speed and mass flow rate. In addition, according to aforementioned T/C turbine simulation approach, T/C turbine efficiency depends on its expansion ratio, which is directly related to T/C speed. Hence, the reduction of T/C turbine expansion ratio mainly at 50% and 75% load due to engine operation with the electric power generation system results in reduction of T/C turbine efficiency compared to conventional engine operation and through that, in reduction of T/C turbine generated torque and T/C shaft rotational speed (see Fig. 6 below). The curtailment of T/C speed results in moderate reduction of charge air mass flow rate through the pertinent reduction of boost pressure (see Fig. 7a) leading thus, to the improvement of compressor efficiency since less shaft power is required for attaining the same compression power.

The increase of power turbine speed results in reduction of T/C turbine efficiency whereas, the corresponding effect on compressor efficiency is negligible at all loads examined. Compressor efficiency is constant and equal to 76.5%, 77% and 77.5% at 100%, 75% and 50% engine load respectively. The maximum decrease of T/C turbine efficiency is approximately 2% and it is observed at partial engine load. The reduction of T/C turbine efficiency with increasing power turbine speed can be ascribed to the reduction of T/C turbine expansion ratio mainly at 50% and 75% load with increasing power turbine speed.

Fig. 5 depicts the variation of power turbine efficiency with its speed. As evidenced, the effect of power turbine speed on its efficiency varies with engine load. Specifically, the power turbine efficiency increases with its speed at full engine load. However, at 75% and 50% engine load, the power turbine efficiency increases initially and starts to reduce after a certain value of power turbine speed. As witnessed from Fig. 5, the maximum value of power turbine efficiency is equal to 79%. In a following paragraph, it will be demonstrated that the values of power turbine speed, which correspond to the maximum observed power turbine efficiency at each examined load correspond also to the maximum bsfc reduction (see Fig. 10 below) revealing thus, a direct relation between power turbine efficiency and bsfc improvement.

5.3. Effect of power turbine speed on turbocharger speed

The influence of power turbine speed on T/C speed is shown in Fig. 6, where the standard case without turbocompounding is also included. As evidenced, the application of electrical turbocompounding on the examined HD diesel engine results in reduction of T/C speed at all loads examined. This observation can be attributed to the aforementioned reduction of T/C turbine efficiency mainly at 50% and 75% load (Fig. 4), which was acknowledged during engine operation with the turbocompounding system compared to the standard operational case. The maximum reduction of T/C speed due to the use of turbocompounding technology is almost 5 krpm. The increase of power turbine speed results in the deterioration of the deviation of the T/C speed from its pertinent value during standard engine operation at all loads examined. This is ascribed to the moderate decline of the T/C speed with

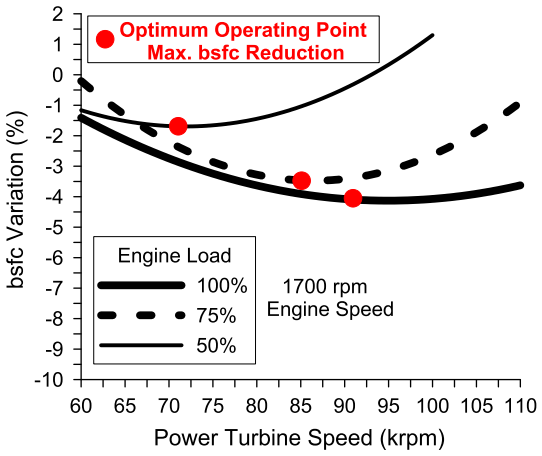

Fig. 10. Effect of power turbine speed on bsfc percentage variation with reference to standard engine operation without turbocompounding. Predictions are given for an electrically turbocompounded HD diesel truck engine at 1700 rpm and at 100%, 75% and 50% of full engine load.

increasing rotational speed of the power turbine. The previous T/C speed reduction with increasing power turbine speed is higher at part engine loads compared to the operation of the system at full engine load. As shown in Fig. 6, the T/C speed decreases from 91.20 krpm to 88.00 krpm at full engine load. Furthermore, the T/C speed is reduced from 83.50 krpm to 78.50 krpm at 75% engine load and from 74.40 krpm to 69.20 krpm at 50% engine load.

According also to Fig. 6, the T/C speed increases with engine load both for turbocompounded and non-turbocompounded diesel engine operation. This is attributed to the increase of thermal energy of exhaust gases, which expand in T/C turbine, due to the increase of fuel injected quantity with increasing engine load. Thus, the higher thermal energy of expanding exhaust gases increases the kinetic energy of T/C turbine blades resulting thus, in an increase of T/C speed.

5.4. Effect of power turbine speed on boost pressure and on air to fuel ratio

A major advantage of the simulation model used in the present analysis is its ability to predict the effect of turbocompounding application on engine boost pressure and air to fuel ratio. For the turbocompounded diesel engine, the impact of power turbine speed on engine boost pressure is given in Fig. 7a. Furthermore, the values of boost pressure for the standard engine without turbocompounding are included in Fig. 7a. As observed, the application of an electrical turbocompounding system to the examined HD diesel engine results in limited reduction of average boost pressure at all loads considered. The lower boost pressures, which were observed in the case of electrical turbocompounding compared to conventional diesel operation, can be attributed to the aforementioned reduction of T/C speed (Fig. 6) as a result of the reduction of T/C turbine efficiency mainly during part load engine operation. The deviation between boost pressure values for the operational case with electrical turbocompounding and the corresponding values for the standard operational case increases with increasing power turbine speed at all loads examined. The aforementioned deviation is more pronounced at part engine loads following the influence of power turbine speed on T/C speed (Fig. 6). As evidenced from Fig. 7a, the maximum decrease of boost pressure caused by the application of turbocompounding technique is rather limited and is equal to 0.2 bar.

According to Fig. 7b, the aforementioned reduction of boost pressure, which was observed in the case of engine operation with electrical turbocompounding system compared to the standard case (Fig. 7a), results in reduction of air to fuel ratio at all loads examined. Hence, the operation of the proposed turbocompounding system downplays the in-cylinder air availability affecting thus negatively the combustion efficiency.

The deviation of air fuel ratios between the case of turbocompounded engine operation and conventional diesel operation increases moderately with increasing power turbine speed at all loads considered following the aforementioned effects of power turbine speed on T/C turbine efficiency, T/C speed and boost pressure. The maximum reduction of air to fuel ratio with respect to standard operational case is 2.5 and is observed at 50% load.

5.5. Effect of power turbine speed on exhaust temperature at T/C turbine inlet (high-pressure exhaust manifold), on power turbine inlet (low-pressure exhaust manifold) and on power turbine outlet

Fig. 8a illustrates the influence of power turbine speed on the average exhaust temperature at the entrance of the T/C turbine and at power turbine inlet. Theoretical results are also given for the mean values of exhaust temperature at the entrance of the T/C turbine, which were considered for diesel engine operation without turbocompounding (standard case) at all loads examined. As observed, the application of the proposed electric power generation system results in significant increase of exhaust gas temperature at T/C turbine inlet compared to conventional diesel operation due to the aforementioned deterioration of air to fuel ratio and the subsequent exacerbation of combustion efficiency. The average increase of exhaust gas temperature at T/C turbine inlet between electrical turbocompounding and conventional diesel operational mode is approximately 103.5 °C, 90 °C and 74 °C at 100%, 75% and 50% load respectively.

As witnessed from Fig. 8a, exhaust gas temperatures both at T/C turbine inlet and power turbine inlet increase with increasing power turbine speed at all loads examined. This is attributed to the aforementioned deterioration of air to fuel ratio (Fig. 7b) with increasing power turbine speed, which results in exacerbation of fuel combustion efficiency and thus, to the increase of exhaust gas temperature at the entrance of T/C turbine and subsequently, to power turbine inlet. It is noteworthy to mention that the temperature drop during the expansion at T/C turbine ranges from 75 °C to 124 °C.

The relative influence of power turbine speed on the average exhaust temperature at the power turbine exit is presented in Fig. 8b. The average temperature drop during the exhaust gas expansion at the power turbine ranges from 68 °C to 131 °C. As witnessed, there is a considerable temperature rise at the exit of the power turbine with its increasing speed. Specifically, the increase of exhaust gas temperature with increasing power turbine speed varies from 32 °C at 100% load to 42 °C at 50% load. The load-dependent effect of power turbine speed on its outlet gas temperature can be related to the pertinent load-contingent variation of power turbine efficiency with its rotational speed, which is already shown in Fig. 5.

5.6. Effect of power turbine speed on generated electric power and on net engine power

The variation of the generated electric power with power turbine speed is shown in Fig. 9a. As observed, the gains in generated electric power are enhanced with increasing engine load due to the higher thermal energy availability of exhaust gases, which expand in the power turbine. The increase of power turbine speed results in a continuous increase of generated electric power at full load. At 75% load, produced electric power initially increases with increasing power turbine speed up to a certain value and then

starts to decline returning back almost to its initial value. In the case of 50% load, the influence of power turbine speed on generated electric power is rather imperceptible. Observed variations of the power turbine speed effect on produced electric power with engine load can be related to pertinent variations, which were observed in the case of power turbine efficiency in Fig. 5. It is noteworthy to mention that the maximum generated electric power is 62 kW, 39 kW and 23 kW at 100%, 75% and 50% of full engine load respectively.

According to Fig. 9b, the application of electrical turbocompounding technology to the examined HD diesel, results in significant reduction of net diesel engine power. This is ascribed to the negative effect of electrical turbocompounding operation on engine average air to fuel ratio, which, as already discussed (Fig. 7b), results in deterioration of diesel combustion efficiency. This reduction varies with engine load and power turbine speed. The highest reductions of net engine power observed at 50% and 100% load reaching up to 15%.

5.7. Effect of power turbine speed on bsfc improvement

The impact of power turbine speed on total bsfc improvement is shown in Fig. 10 at all loads considered in this study. At all loads, the positive effect of the applied turbocompounding technology on bsfc relative reduction is enhanced with increasing power turbine speed up to a certain point and then, is curtailed. Thus, the previous value of power turbine speed corresponds to the optimum operating point of the examined turbocompound engine. As witnessed, the optimum value of power turbine speed increases with the engine load. The maximum bsfc improvement is 4.1%, 3.1% and 2%, when the engine load is 100%, 75% and 50% respectively and the corresponding values of power turbine speed are equal to 90 krpm, 85 krpm and 70 krpm. As revealed from Fig. 10, the operation of power turbine at high speed values could cause a deterioration of bsfc at part engine load. Thus, power turbine speed is limited at 100 krpm for 50% engine load. The variation of bsfc improvement with power turbine speed and engine load is directly related to the pertinent effects of power turbine speed and load on power turbine efficiency (Fig. 5) and through that on generated electric power (Fig. 9a) and on net engine power (Fig. 9b). Specifically, as already mentioned in the discussion of Fig. 5, the power turbine efficiency increases with power turbine speed at full load whereas, at 50% and 75% load this increase is limited up to a certain optimum power turbine speed. These effects were transferred in the case of variation of generated electric power with power turbine speed at each load examined. Hence, the increase of generated electric power with increasing power turbine speed is counterbalanced by the corresponding reduction of net engine power. For this reason, there is a certain optimum power turbine speed at each load at which the bsfc improvement is maximized because possibly up to this point the positive effects of power turbine speed on generated electric power overwhelms the pertinent negative influence on net engine power. For values of power turbine speed higher than the optimum one at each load, the balance between the increased electric power and the decreased net engine power does not support further improvement of bsfc.

6. Conclusions

The parametric investigation of the present analysis was based on an engine simulation model using operating charts provided by the manufacturer for turbocharger components and power turbine. A novel approach was employed for the simulation of T/C compressor, T/C turbine and power turbine using the aforementioned operational charts. Power turbine speed was used as varying parameter in the theoretical analysis performed in the present study. The assessment of the theoretical results, which were generated in this study, led to the consolidation of the following concluding remarks:

- The application of electrical turbocompounding technology on a HD diesel truck engine resulted in significant increase of engine back-pressure (i.e. mean exhaust pressure in the manifold between engine and T/C turbine) compared to standard engine operation. Deviations of exhaust back-pressure with respect to conventional operation ranged from 1.26 bar at 50% load to 2.84 bar at 100% load. The effect of increasing power turbine speed on exhaust back-pressure variation was imperceptible.
- The increase of power turbine speed resulted in an increase on exhaust pressure at power turbine inlet and thus, on its expansion ratio at all loads examined. The average value of power turbine expansion ratio ranged from 1.7 at 50% load to 2.4 at full load.
- The implementation of mechanically-powered electric generator in a HD diesel truck engine resulted in an increase of compressor efficiency and in a decrease of T/C turbine efficiency. T/C turbine efficiency was further slightly reduced with increasing power turbine speed whereas compressor efficiency remained almost unaffected by the variation of power turbine speed.
- The power turbine efficiency increases with its speed at full load whereas, at part load engine operation, the increase of power turbine efficiency is limited up to certain optimum values of its speed. The maximum value of power turbine efficiency is equal to 79%.
- The installation of a power turbine downstream to T/C turbine resulted in reduction of T/C shaft speed compared to standard diesel operation at all loads examined. This reduction was enhanced with increasing power turbine speed.
- The application of electrical turbocompounding technology on a HD diesel truck engine resulted in limited reduction of boost pressure and subsequently, in reduction of average air to fuel ratio. The deviations of boost pressure and air to fuel ratio, which were observed in the case of electrical turbocompounding compared to standard case increased with increasing power turbine speed. The highest reduction of boost pressure, which was induced by the application of turbocompounding concept, was 0.2 bar.
- The operation of an electric power generation turbine downstream to a HD diesel engine T/C resulted in significant elevation of the mean exhaust temperature at the entrance of T/C turbine compared to standard diesel operation. The exhaust gas temperature rise at T/C turbine inlet due to the turbocompounding system operation was ranged from 74 °C at 50% load to 103.5 °C at 100% load. In addition, the increase of power turbine speed resulted in the increase of average exhaust temperatures at T/C turbine inlet and power turbine inlet as a result of the reduction of air to fuel ratio. Increasing power turbine speed results in an increase of exhaust temperature after power turbine at all operating cases examined.
- Generated electric power increases with increasing power turbine speed at full load. At 50% and 75% load the increase of electric power is limited up to certain optimum values of power turbine speed. These variations are in accordance with the pertinent variations of power turbine efficiency. The highest value of produced electric power was 62 kW at full load.
- The net engine power is negatively affected by the installation of electric power generating system. This hazardous effect is more pronounced at 50% and 100% load reaching up to 15% at the highest power turbine speed considered herein.

- The implementation of electric turbocompounding strategy in a HD diesel truck engine results in noticeable bsfc improvements, which were observed for different optimum power turbine speeds at each load considered. The maximum bsfc reduction achieved was 4.1% at full load and the lowest was 2% at 50% load.

Overall, it can be stated that the installation of a power turbine coupled with an electric generator downstream to the T/C turbine is an attractive solution for significantly reducing diesel engine specific fuel consumption using exhaust gas heat recovery. It must be underlined that the aforementioned bsfc improvement can be attained in the case of electrical turbocompounding mainly with lower technical complexity and installation cost against other competitive WHR technologies such as the Rankine cycle system. Further bsfc improvement may be experienced if a more efficient power turbine is employed with the turbocompounding system by considering also the implications of turbocompounding technology on engine air supply, which is primarily affected by the difference between charge pressure and exhaust back-pressure.

Acknowledgements

The authors would like to express their gratitude to the European Union for supporting financially the project "GREEN" (TIP4-CT-2005-516195) under which the current investigation has been conducted. Also they would like to express their gratefulness to IVECO for providing valuable experimental data for the validation of the simulation model and to HOLSET for supplying the T/C maps used in this study.

References

[1] Dec JE. Advanced compression-ignition engines—understanding the in-cylinder processes. Proc Combust Inst 2009;32:2727–42.
[2] Reitz RD. Directions in internal combustion engine research. Combust Flame 2013;160:1–8.
[3] Binder K, Schwarz V. Present and future of heavy duty engine strategies for compliance to the emission legislation. In: Conference of Thermo- and Fluid Dynamic Processes in Diesel Engines (THIESEL), Valencia, Spain; 2002.
[4] Hountalas DT, Mavropoulos GC, Zannis TC, Schwarz V. Possibilities to achieve future emission limits for HD DI diesel engines using internal measures. SAE paper no. 2005-01-0377; 2005.
[5] Hountalas DT, Kouremenos DA, Pariotis EG, Schwarz V, Binder KB. Using a phenomenological multi-zone model to investigate the effect of injection rate shaping on performance and pollutants of a DI heavy duty diesel engine, SAE paper no. 2002-01-0074; 2002.
[6] Wickman DD, Senecal PK, Tanin KV, Reitz RD, Gebert K, Barkhimer RL, Beck NJ. Methods and results from the development of a 2600 bar diesel fuel injection system. SAE paper no. 2000-01-0947; 2000.
[7] Hountalas DT, Mavropoulos GC. Potential for improving HD diesel truck engine fuel consumption using exhaust heat recovery techniques in Joo Er M (ed.), New trends in technologies: devices, computer, communication and industrial systems, InTech; 2010.
[8] Sprouse III C, Depcik C. Review of organic Rankine cycles for internal combustion engine exhaust waste heat recovery. Appl Therm Eng 2013;51:711–22.
[9] Saidur R, Rezaei M, Muzammil WK, Hassan MH, Paria S, Hasanuzzaman M. Technologies to recover exhaust heat from internal combustion engines. Renew Sustain Energy Rev 2012;16:5649–59.
[10] Wang T, Zhanga Y, Peng Z, Shu G. A review of researches on thermal exhaust heat recovery with Rankine cycle. Renew Sustain Energy Rev 2011;15:2862–71.
[11] Shu G, Liang Y, Wei H, Tian H, Zhao J, Liu L. A review of waste heat recovery on two-stroke IC engine aboard ships. Renew Sustain Energy Rev 2013;19:385–401.
[12] Hountalas DT, Katsanos CO, Mavropoulos GC. Efficiency improvement of large scale 2-stroke diesel engines through the recovery of exhaust gas using a Rankine cycle. Procedia – Soc Behav Sci 2012;48:1444–53.
[13] Katsanos CO, Hountalas DT, Pariotis EG. Thermodynamic analysis of a Rankine cycle applied on a diesel truck engine using steam and organic medium. Energy Convers Manage 2012;60:68–76.
[14] Yu G, Shu G, Tian H, Wei H, Liu L. Simulation and thermodynamic analysis of a bottoming Organic Rankine Cycle (ORC) of diesel engine (DE). Energy 2013;51:281–90.
[15] Weerasinghe WMSR, Stobart RK, Hounsham SM. Thermal efficiency improvement in high output diesel engines: a comparison of a Rankine cycle with turbo-compounding. Appl Therm Eng 2010;30:2253–6.
[16] Leising CJ, Purohit GP, DeGrey SP, Finegold JG. Waste heat recovery. SAE paper no. 780686; 1978.
[17] Brands MC, Werner J, Hoehne JL. Vehicle testing of Cummins turbocompound diesel engine. SAE paper no. 810073; 1981.
[18] Kamo R, Brysik W. Adiabatic turbocompound engine performance prediction. SAE paper no. 780068; 1978.
[19] Tennant DWH, Walsham BE. The turbocompound diesel engine. SAE paper no. 89064; 1989.
[20] Wilson DE. The design of a low specific fuel consumption turbocompound engine. SAE paper no. 860072; 1986.
[21] Hountalas DT, Katsanos CO, Kouremenos DA, Rogdakis ED. Study of available exhaust gas heat recovery technologies for HD diesel engine applications. Int J Altern Propul 2007;1:228–49.
[22] Sendyka B, Soczowka J. Recovery of exhaust gases energy by means of turbocompound. Politechnika Krakowska; 2001.
[23] Boretti A. Conversion of a heavy duty truck diesel engine with an innovative power turbine connected to the crankshaft through a continuously variable transmission to operate compression ignition dual fuel diesel-LPG. Fuel Process Technol 2013;113:97–108.
[24] Hountalas DT, Katsanos CO, Lamaris VT. Recovering energy from the diesel engine exhaust using mechanical and electrical turbocompounding. SAE paper no. 2007-01-1563; 2007.
[25] Hopmann U. Diesel engine waste heat recovery utilizing electric turbocompound technology. In: Catterpillar, Directions in Engine-Efficiency and Emissions Research (DEER) conference, San Diego, California, USA; 2004.
[26] Hopmann U, Algrain M. Diesel engine waste heat recovery utilizing electric turbocompound technology. Caterpillar Inc., Directions in Engine-Efficiency and Emissions Research (DEER) Conference, Newport, Rhode Island, USA; 2003.
[27] Di Nanno LR, Di Bella FA, Koplow MD. An RC-1 organic Rankine bottoming cycle for an adiabatic diesel engine. Thermoelectron Corp., Master Thesis, Waltham, MA, USA; 1983.
[28] Di Bella FA, Di Nanno LR, Koplow MD. Laboratory and on-highway testing of diesel organic Rankine compound long-haul vehicle engine. SAE paper no. 830122; 1983.
[29] Doyle E, Di Nanno LR, Kramer S. Installation of a diesel-organic Rankine compound engine in a class 8 truck for a single-vehicle test. SAE paper no. 790646; 1979.
[30] Parimal PS, Doyle DF. Compounding the truck diesel engine with an organic Rankine cycle system. SAE paper no. 760343; 1976.
[31] Sekar R, Cole RL. Integrated Rankine bottoming cycle for diesel truck engines. Argonne National Laboratory. Master Thesis; 1987.
[32] Teng H, Regner G, Cowland C. Waste heat recovery of heavy-duty diesel engines by organic Rankine cycle Part I: Hybrid energy system of diesel and Rankine engines. SAE paper no. 2007-01-0537; 2007.
[33] Teng H, Regner G, Cowland C. Waste heat recovery of heavy-duty diesel engines by organic Rankine cycle Part II: Working fluids for WHR-ORC. SAE paper no. 2007-01-0543; 2007.
[34] Teng H, Regner G. Improving fuel economy for HD diesel engines with WHR Rankine cycle driven by EGR cooler heat rejection. SAE paper no. 2009-01-2913; 2009.
[35] Teng H, Klaver J, Park T, Hunter GL, van der Velde B. A Rankine cycle System for recovering waste heat from HD diesel engines – WHR system development. SAE paper no. 2011-01-0311; 2011.
[36] Park T, Teng H, Hunter GL, van der Velde B, Klaver J. A Rankine cycle system for recovering waste heat from HD Diesel Engines – Experimental results. SAE paper no. 2011-01-1337; 2011.
[37] Dolz V, Novella R, Garcia A, Sanchez J. HD Diesel engine equipped with a bottoming Rankine cycle as a waste heat recovery system. Part 1: study and analysis of the waste heat energy. Appl Therm Eng 2012;36:269–78.
[38] Serrano JR, Dolz V, Novella R, Garcia A. HD Diesel engine equipped with a bottoming Rankine cycle as a waste heat recovery system. Part 2: evaluation of alternative solutions. Appl Therm Eng 2012;36:279–87.
[39] Hountalas DT, Mavropoulos GC, Katsanos CO, Knecht W. Improvement of bottoming cycle efficiency and heat rejection for HD truck applications by utilization of EGR and CAC heat. Energy Convers Manage 2012;53:19–32.
[40] Koeberlein D. Supertruck technologies for 55% thermal efficiency and 68% freight efficiency. In: Directions in Engine-Efficiency and Emissions Research (DEER) conference, Dearborn, Michigan, USA; 2012.
[41] De Ojeda W. Development and demonstration of a fuel-efficient HD engine. In: Directions in Engine-Efficiency and Emissions Research (DEER) conference, Dearborn, Michigan, USA; 2012.
[42] Bass JC, Kushch AS, Elsner NB. Thermoelectric generator (TEG) on heavy diesel trucks. Hi-Z Technology Inc; 2002.
[43] Kushch AS, Bass JC, Ghamaty S, Elsner NB. Thermoelectric development at Hi-Z technology. Hi-Z Technology Inc; 2002.
[44] Rakopoulos CD, Hountalas DT. Development and validation of a 3-D multi-zone combustion model for the prediction of a DI diesel engines performance and pollutants emissions. SAE Trans J Eng 1998;107:1413–29.
[45] Annand WJD. Heat transfer in the cylinders of reciprocating internal combustion engines. Proc Inst Mech Eng 1963;177:973–90.
[46] Heywood JB. Internal combustion engine fundamentals. McGraw-Hill; 1988.

[47] Dent JC, Derham JA. Air motion in a four-stroke direct injection diesel engine. Proc Inst Mech Eng 1974;188:269–80.
[48] Nishida K, Hiroyasu H. Simplified three-dimensional modeling of mixture formation and combustion in a DI diesel engine. SAE paper no. 890269; 1989.
[49] Jung D, Assanis DN. Multi-zone DI diesel spray combustion model for cycle simulation studies of engine performance and emissions. SAE paper no. 2001-01-1246; 2001.
[50] Ramos JI. Internal combustion engine modeling. Hemisphere; 1989.
[51] Borman GL, Johnson JH. Unsteady vaporization histories and trajectories of fuel drops injected into swirling air. SAE paper no. 598C, National Powerplant Meeting, Philadelphia (PA); 1962.
[52] Kadota T, Hiroyasu H, Oya H. Spontaneous ignition delay of a fuel droplet in high pressure and high temperature gaseous environments. Bulletin JSME 1976;19(130).
[53] Watson N, Janota MS. Turbocharging the internal combustion engine. Macmillan Press; 1982.